



NRC Publications Archive Archives des publications du CNRC

Effects of strip temperature and Mn content on galvanizing bath management

Yu, K. R.; Ilinca, F.; Goodwin, F. E.

This publication could be one of several versions: author's original, accepted manuscript or the publisher's version. / La version de cette publication peut être l'une des suivantes : la version prépublication de l'auteur, la version acceptée du manuscrit ou la version de l'éditeur.

Publisher's version / Version de l'éditeur:

Galvanizers Association Proceedings 2017, 2017-10-16

NRC Publications Record / Notice d'Archives des publications de CNRC:

<https://nrc-publications.canada.ca/eng/view/object/?id=28016e33-3b97-4e95-9d7e-58b3411dd511>
<https://publications-cnrc.canada.ca/fra/voir/objet/?id=28016e33-3b97-4e95-9d7e-58b3411dd511>

Access and use of this website and the material on it are subject to the Terms and Conditions set forth at

<https://nrc-publications.canada.ca/eng/copyright>

READ THESE TERMS AND CONDITIONS CAREFULLY BEFORE USING THIS WEBSITE.

L'accès à ce site Web et l'utilisation de son contenu sont assujettis aux conditions présentées dans le site

<https://publications-cnrc.canada.ca/fra/droits>

LISEZ CES CONDITIONS ATTENTIVEMENT AVANT D'UTILISER CE SITE WEB.

Questions? Contact the NRC Publications Archive team at

PublicationsArchive-ArchivesPublications@nrc-cnrc.gc.ca. If you wish to email the authors directly, please see the first page of the publication for their contact information.

Vous avez des questions? Nous pouvons vous aider. Pour communiquer directement avec un auteur, consultez la première page de la revue dans laquelle son article a été publié afin de trouver ses coordonnées. Si vous n'arrivez pas à les repérer, communiquez avec nous à PublicationsArchive-ArchivesPublications@nrc-cnrc.gc.ca.



Galvanizers Association Annual Conference 2017
Troy, MI
October 15-18, 2017

Effects of Strip Temperature and Mn content on Galvanizing Bath Management

K. R. Yu¹, F. Ilinca¹, F. E. Goodwin²

¹ National Research Council of Canada
75 de Mortagne, Boucherville, Québec, Canada. J4B 6Y4
Phone: (450) 641-5072
Email: florin.ilinca@cnrc-nrc.gc.ca; kintakraymond.yu@cnrc-nrc.gc.ca

² International Zinc Association
2530 Meridian Parkway, Ste. 115, Durham, NC 27713
Phone: (919) 361-4647
Email: fgoodwin@zinc.org

Effects of Strip Temperature and Mn content on Galvanizing Bath Management

K. R. Yu, F. Ilinca, F. E. Goodwin

ABSTRACT

Achieving a stable thermal field and adequate control of aluminum and iron content in continuous galvanizing bath operations are of critical importance in achieving automotive quality coated steel products. Previously, numerical models have been developed to describe the flow, temperature and compositional variations in a conventional continuous galvanizing operation. For advanced high strength steels, the strip entry temperature can be different from the mean bath temperature because of over-aging treatments such as carbon partitioning or bainitic transformation that are performed just before entry into the zinc bath. Moreover, advanced high strength steels typically have higher manganese content, which may dissolve into the bath. It is anticipated that the elevated Mn content of the strip could also potentially influence the bath dross formation. This work aims to numerically examine the effects of these two aspects, namely a strip entering the bath at a temperature different from the bath temperature and the Mn content of the strip, on the bath dross formation.

To investigate the effect of strip entry temperature, five different strip temperatures are considered from 420 to 500°C for both the GA and GI conditions. The averaged bath temperature is maintained at 460°C. A gradual aluminum ingot melting scheme is employed to simplify the analysis. Temperature dependent iron dissolution and aluminum uptake rates of the strip are considered. As for the influences of the Mn content of the strip, a parametric study is performed at three strip Mn compositions and three strip temperatures, again for both the GA and GI conditions. For each scenario, the temperature and compositional profiles as well as the dross formation patterns of the bath are compared at 12 locations in the snout, sink roll and the inductor-ingot loading regions with those of the mean average values.

Different strip entry temperatures result in different bath temperature distributions, and lead to different dross formation patterns. Low dross formation is observed at the location where the local temperature is high; and vice versa. Due to the higher iron dissolution rate of the strip and different intermetallic phases formed at the low bath aluminum level, more dross is developed at the GA condition. However, the effects of strip temperatures are similar for both the GA and GI conditions. Due to the difference in iron substitution rates with manganese for the different intermetallic species, it is expected that higher strip Mn content could lead to higher dross formation at the GA condition, but not for the GI condition.

It is concluded that local bath temperature must be properly regulated to minimize the local dross formation. Higher strip entry temperature will result in much less dross around the strip, but it may still lead to higher overall dross formation. Aside, higher strip entry temperature requires less power to maintain the overall energy balance of the bath and may be beneficial for energy consumption reduction. On the other hand, higher strip Mn content could result in significantly more dross, particularly at the GA condition. Lastly, the iron dissolution rate from the steel strip has great impacts on the dross formation and such factor should be carefully considered in the bath management analysis.

Effects of Strip Temperature and Mn content on Galvanizing Bath Management

K. R. Yu, F. Ilinca, F. E. Goodwin

Keywords: Dross formation, Continuous Galvanizing Bath, Numerical modeling, Strip Entry Temperature, Mn content

INTRODUCTION

Recently, advanced high strength steels (AHSS) have become popular in the automotive industry due to their unique combined light weight and high strength characteristics. These desired properties are obtained from proper addition of alloying elements and carefully controlled heat treatments [1]. The strip entry temperature of AHSS can be different from the mean bath temperature because of over-aging treatments such as carbon partitioning or bainitic transformation that are performed just before entry into the zinc bath. Such temperature differences may have a substantial impact on the bath thermal field. A local decrease in the bath temperature reduces the solubility of both Fe and Al in the bath, which in turn promotes the formation of dross particles. Moreover, advanced high strength steels typically have higher Mn content, which may dissolve into the bath. It is anticipated that the elevated Mn content of the strip could also potentially influence the bath dross formation. It is well-known that dross formation is a major obstacle in the production of high quality galvanizing coating [2]. Therefore, it is needed to better understand the potential impacts of these two aspects, namely a steel strip entering the galvanizing bath at a temperature different from the bath temperature and the Mn content of the strip, on the bath dross formation.

Numerical simulation has been shown to be a valuable tool to examine the characteristics of the flow field of the galvanizing bath. A three-dimensional numerical model had previously been developed to determine the flow, temperature and compositional characteristics for various galvanizing bath operations [3]–[6]. The galvanizing bath model had been validated against real-time plant data for a complex transition process from galvanneal (GA) to galvanizing (GI) operations [7]. The simulation results and the plant data are in excellent agreement.

The present work is in two parts. First, to further characterize the effect of the strip entry temperature difference, a parametric study is performed based on previous work [8]. Five different strip entry temperatures from 420 to 500°C are considered for more realistic operations at both the GA and GI conditions. The case of $T_{strip} = 460^{\circ}\text{C}$, which is the same as the typical mean bath temperature, is set as reference in the comparison. After, to evaluate the influences of the Mn content of the strip, a similar parametric study is carried at three strip Mn compositions (0.0, 6.0 and 15 wt%) and three strip temperatures (440, 460 and 480°C), again for both the GA and GI conditions.

The paper is organized as follows: First, the numerical model for the galvanizing bath is described. The methodology for the numerical experiment is then explained. After, the results for the effects of the strip entry temperature are presented and discussed, followed by those for the effects of the Mn content. The findings are summarized in the conclusion.

NUMERICAL MODEL

Overview of the galvanizing bath model

The configuration of a typical 250 ton galvanizing bath is shown in Figure 1 **Error! Reference source not found.**. The steel strip enters the galvanizing bath through the snout region. It turns

around the sink roll and exits the molten zinc bath directed by a set of guide rolls. Al is often added to the zinc bath to control growth of the interface layer [9]. A thin (generally $< 1 \mu\text{m}$) inhibition layer of Fe_2Al_5 is formed on the surface of the strip. Zn-Al ingots are added to the bath to regulate bath composition, where the inductor provides the required energy for ingot melting. In the model, the heating rate of the inductor can be adapted to reflect the different ingot loading cycles.

Besides the heating from the inductor, the overall heat balance also considers the heat losses through the side walls, the top and bottom surfaces of the bath. Furthermore, operating parameters such as line speed, strip width, and strip temperature can be adjusted in the model.

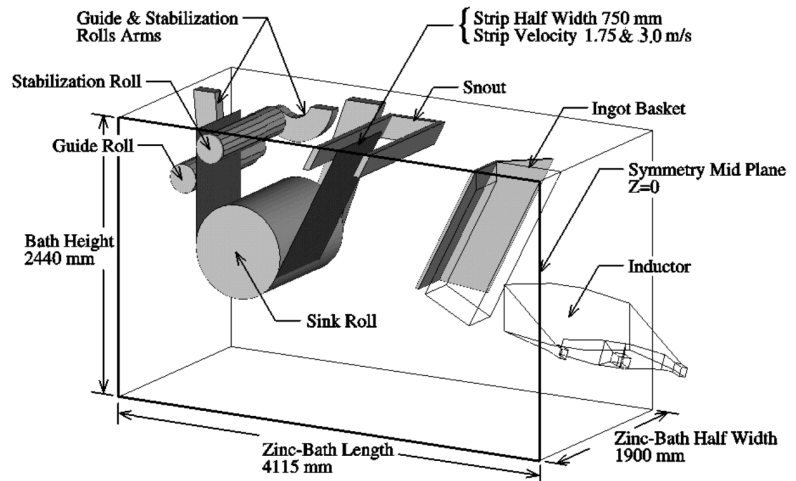


Figure 1: A typical galvanizing bath configuration (half of the bath width shown)

Governing equations and analytical model

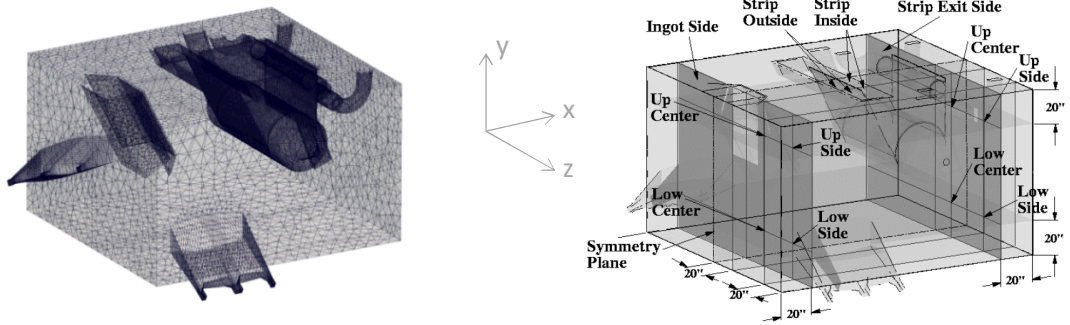
The molten liquid zinc alloy is modeled as an incompressible Newtonian fluid. The turbulent bath flow is determined using the standard $k - \varepsilon$ turbulence model in the positivity preserving logarithmic form [10]. The buoyancy effects are considered using the Boussinesq approximation. The mass balance of the solute concentrations of (Fe, Mn) and Al are described by the convection-diffusion equations. The formation of intermetallic dross particles is determined by the solubility limit of the solute components indicated by the phase diagram of the alloy system and depends on the local solute concentrations and the bath temperature [11], [12].

The melting of the ingots is modeled in the energy and mass transport equations using flux boundary conditions at the ingot/bath interface; meanwhile the (Fe, Mn) and Al dissolution and consumption are implemented as flux boundary conditions respectively on the strip surface in the strip entry region.

It is assumed that the formation/dissolution of dross precipitates occurs instantaneously, and that any new addition of solute components results in the nucleation of dross particles when the total solute concentration exceeds the solubility limit of the specific composition of the bath. Besides, the dross particles are assumed to be sufficiently small that they have negligible influences on the molten Zn flow. Also, no agglomeration of the dross particles occurs during their movements in the bath. Past simulations, based on these assumptions, have successfully demonstrated the sensitivity of dross formation to temperature variations.

The governing equations are discretized using a finite element method. In particular, the Navier-Stokes and the scalar transport equations are solved using a streamline-upwind Petrov-Galerkin (SUPG) approach [13]. The resulting global system of equations is solved in a partly segregated manner [7].

For further information regarding the galvanizing bath model, the reader is referred to Ilinca et al. [7]. Note that the galvanizing bath configuration considered in the present study does not have the wall heating feature.



a) Mesh: # of nodes 315,831,
of elements 1,801,085

b) Sampling locations for field properties.

Figure 2: Computational domain, full bath shown

Computational domain

The computational domain is discretized using four-node tetrahedral elements with a mesh of 315,831 nodes and 1,801,085 elements, shown in Figure 2a. The system of equations is solved in parallel using a Beowulf cluster.

METHODOLOGY

Simulations are performed for a two-hour operation period for each test condition considered. The case of $T_{strip} = 460^{\circ}\text{C}$, which is the same as the typical galvanizing bath temperature, is selected as reference. The overall temperature distribution, solute concentrations and the dross formation characteristics are examined, as well as those at 12 specifically chosen locations in the bath (**Error! Reference source not found.**Figure 2b). The coordinates of selected locations are listed in Table 1.

Table 1: Sampling locations for field properties

Location	Name	X (in/mm)	Y (in/mm)	Z (in/mm)
Ingot Side	Up-Center	-61 / -1549	-20 / -508	20 / 508
	Up-Side	-61 / -1549	-20 / -508	55 / 1397
	Low-Center	-61 / -1549	-76 / -1930	20 / 508
	Low-Side	-61 / -1549	-76 / -1930	55 / 1397
Strip Exit Side	Up-Center	61 / 1549	-20 / -508	20 / 508
	Up-Side	61 / 1549	-20 / -508	55 / 1397
	Low-Center	61 / 1549	-76 / -1930	20 / 508
	Low-Side	61 / 1549	-76 / -1930	55 / 1397
Snout Region	Inside-Center	0 / 0	0 / 0	0 / 0
	Inside-Extremity	-3 / -76	0 / 0	36 / 914

	Outside-Center	-7 / -196	0 / 0	0 / 0
	Outside-Extremity	-3 / -76	0 / 0	-36 / -914

For the present study, a gradual (or continuous) ingot loading scheme is chosen, as opposed to a periodic ingot loading scheme, to minimize the fluctuations of the concentrations of aluminum. This allows closer examinations of the dross formation characteristics. For the present case, Zn-0.5% Al ingot is considered.

Table 2: Parameters for the inductor operations for the considered strip entry temperatures

T_{strip} (°C)	Flow rate	$T_{increase}$ (°C)	Power ¹
420	100%	+15.6	78%
440	100%	+12.5	63%
460	100%	+9.5	48%
480	100%	+6.4	32%
500	100%	+3.5	17%

The difference in the strip entry temperature disturbs the global energy balance of the bath. Prior to the numerical analysis, the parameters for the inductor operations are first adjusted to ensure that the overall mean galvanizing bath temperature is maintained at $T_{bath} = 460^{\circ}\text{C}$ over the two hours operation period. The parameters for the inductor operations for the various strip entry temperatures are listed in Table 2. The overall power input from the inductors and the heat balance of the galvanizing bath for $T_{strip} = 460^{\circ}\text{C}$ are shown in Figure 3 which illustrates that constant overall heat balance is attained.

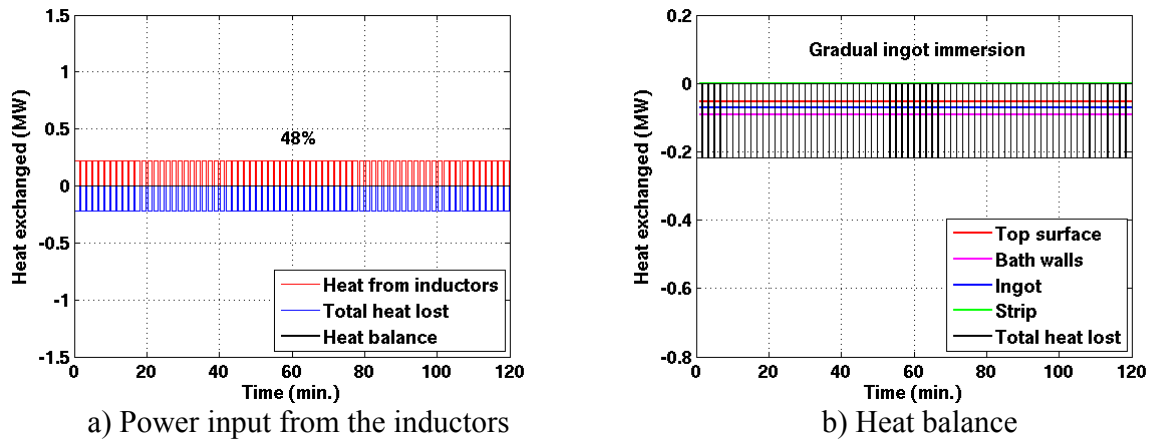


Figure 3: Overall power input and heat balance of the bath for $T_{strip} = 460^{\circ}\text{C}$

Besides the overall heat balance, it is well known that the difference in the strip entry temperature also influences the Fe dissolution and the Al uptake rates of the strip [13]. For each strip entry temperature, these rates are adjusted according to the prediction of the latest update of the well-validated MAP (Modeling Aluminum Pick-up) program from Teck Metals Ltd. [15]. The line speed is set at 105 m/min, and the strip immersion length is 3.12 m. The bath temperature is considered as constant at 460°C and the bath Al content is at around 0.12 wt% for the GA and 0.16 wt% for the GI conditions respectively.

¹ Note that the inductor in the galvanizing bath model is capable to deliver a temperature increase of 20°C at full power.

To examine the effect of strip entry temperature, conventional low carbon steel is considered. In this case, the liquid zinc bath can be described by the well-established zinc-rich corner of the Al-Fe-Zn ternary phase system. To determine the influence of the Mn content in the strip, details of the zinc-rich corner of the Al-Fe-Mn-Zn quaternary phase system must be known. Such data is still very limited. However, the Mn dissolution rate is found to be rather small. Therefore, the ternary phase diagram can be enhanced to describe the Fe solubility limit for the quaternary phase system in the present work. More details will follow.

ON THE EFFECT OF STRIP ENTRY TEMPERATURES

Temperature distribution

The overall temperature distributions in the bath for the five strip entry temperatures are shown in Figure 4. The difference in the strip entry temperature leads to substantial differences in the temperature distribution in the galvanizing bath. The influences can be clearly observed at the snout, sink roll and the ingot loading areas. A cool ingot loading region is observed for all cases due to the continuous ingot loading. The areas above the ingot loading region exhibit an opposite trend with respect to the strip entry temperature. This region receives the flows directly from the inductors. Recall that for a low strip entry temperature, the inductors are required to operate at a higher power to ensure the global energy balance, which results in a higher temperature in this area. The reverse is observed for a high strip entry temperature.

The local temperature profiles² at the 12 selected locations are shown in Figure 5. The results Figure 5 reinforce the observation from Figure 4.

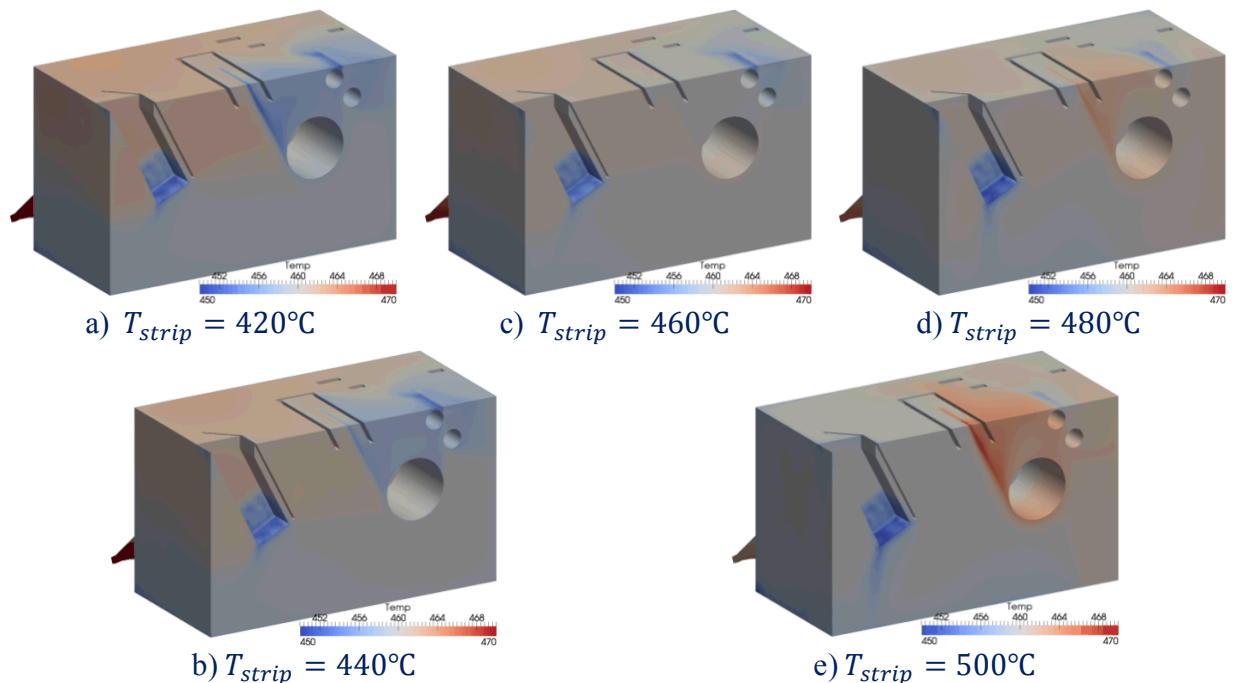


Figure 4: Overall temperature profile for the five strip entry temperatures, half of the bath width shown

² Note that the local temperature profiles at $T_{strip} = 440^{\circ}\text{C}$ are rather similar to those at $T_{strip} = 420^{\circ}\text{C}$. It is likewise for those at $T_{strip} = 480^{\circ}\text{C}$, with respect to the results at $T_{strip} = 500^{\circ}\text{C}$. Hence, they are not shown.

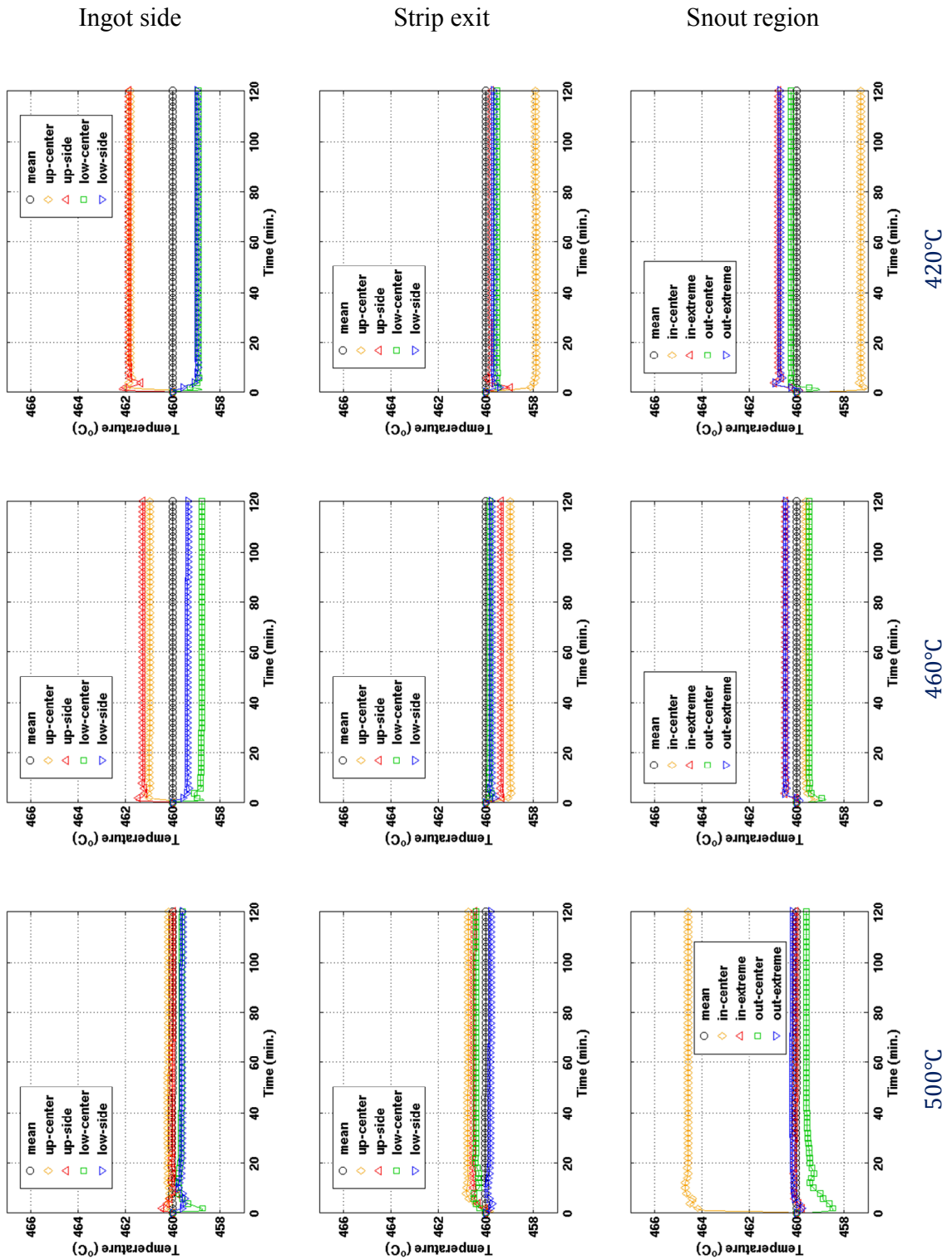


Figure 5: Local temperature profile for the strip entry temperature of 420°C, 460°C and 500°C.

Bath Al and Fe concentration

The evolution of the overall mean Al and Fe concentrations for the gradual ingot melting scheme at five strip entry temperatures at 0.11 wt% [Al] (GA) and 0.16 wt% [Al] (GI) conditions are shown in Figure 6. The mean Al concentrations increase continuously as expected for the gradual ingot melting schemes, respecting the difference in the Al uptake rates. The subtle difference among the five strip entry temperatures is more apparent for the mean Fe concentration than those of the Al. In particular, the MAP program predicts higher Fe dissolution rate with higher strip entry temperature. The continuously increasing mean Al and Fe concentrations lead to constantly increasing dross formation (Figure 6c and Figure 6f).

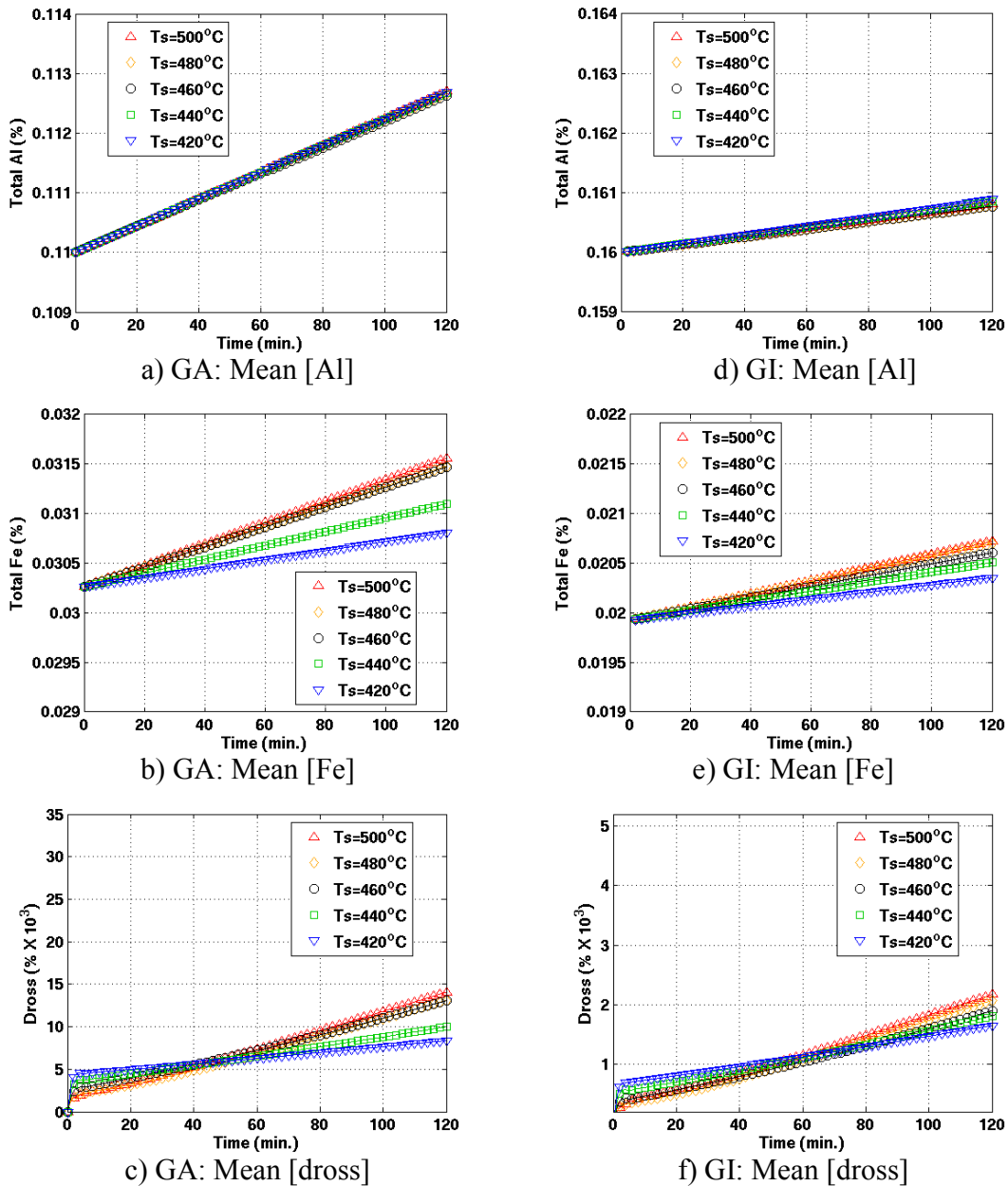


Figure 6: Time evolution of mean [Al], [Fe] and [Dross] with temperature dependent iron dissolution and aluminum up-take rates from the MAP prediction.

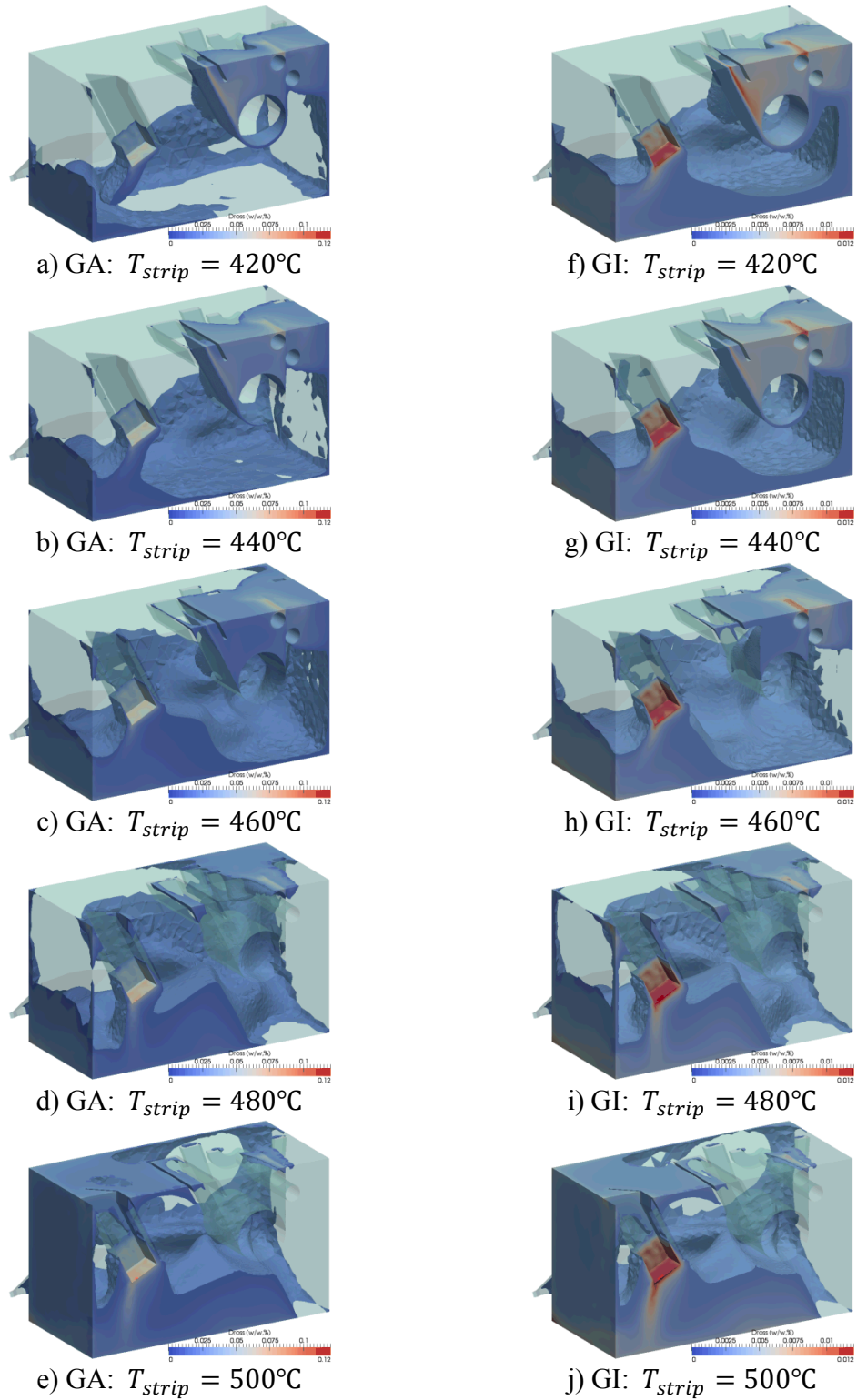


Figure 7: Dross formation characteristics in the bath for the GA and GI conditions at five strip entry temperatures

Dross formation profile

Figure 7 shows the dross formation profiles for the gradual ingot melting scheme with respect to the five different strip entry temperatures for the GA and the GI conditions. The regions of the bath where the dross formation rate is higher than the mean value of the bath at the reference condition are shown. First, very similar overall dross formation patterns can be observed for both the GA and the GI conditions. By comparing the dross formation with the bath temperature profiles in Figure 4 **Error! Reference source not found.**, it can be observed that the dross formation characteristics are generally inversely related to the local bath temperature. More specifically, high dross formation rate is observed wherever the local bath temperature is low, and vice versa. Certainly, the local concentration of the solute elements also has influences on the dross formation. Such effect is best observed by comparing the dross formation between the GA and the GI conditions; in particular for lower strip entry temperatures. Note that the color scale for the GA conditions here is 10 times higher than that for the GI. The reason is that the amount of dross formed for the GA condition is much higher, firstly, because of the higher Fe dissolution rate for the GA condition and secondly, due to the different intermetallic types formed for the two conditions.

The local dross formation profiles at the selected locations for the GA and the GI conditions are shown in Figure 8 and Figure 9. Notice again the high similarity in the dross formation rates at the various locations between the GA and the GI conditions. These results reinforce the observation from the overall dross formation profiles. Note that there are locations where there is no dross formed at the beginning (e.g. the up-center at the ingot region in Figure 8 and Figure 9 for $T_{strip} = 460^{\circ}\text{C}$). These locations correspond to the areas with higher relative temperatures, and thus higher Fe solubility limits. Consequently, the formation of dross is delayed until the solute concentration becomes higher.

The overall bath dross formation rates for the GA and GI conditions are summarized in Table 3. Higher dross formation rate is observed for the higher strip entry temperatures. Recall however that the locations of dross formation are different for the different strip entry temperatures.

Table 3: Bath average dross formation rate for the GA and GI conditions

T_{strip} (°C)	Bath avg. dross (0.11 wt% Al)		Bath avg. dross (0.16 wt% Al)	
	kg	wt%	kg	wt%
420	22.03	9.08e-3	4.17	1.72e-3
440	26.83	1.11e-2	4.64	1.91e-3
460	35.35	1.46e-2	4.96	2.04e-3
480	35.41	1.46e-2	5.35	2.21e-3
500	38.45	1.59e-2	5.59	2.30e-3

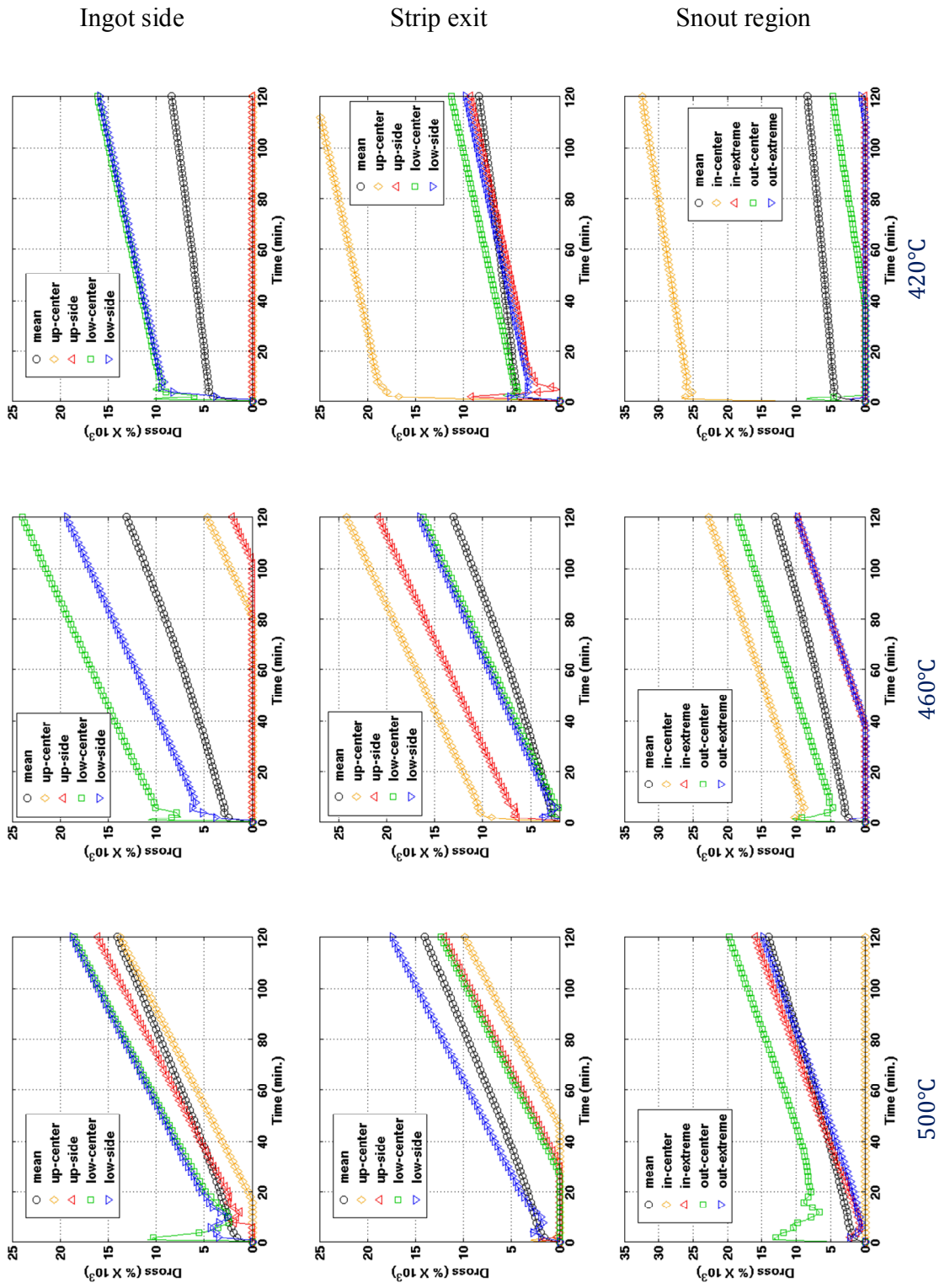


Figure 8: Local dross formation profiles for GA condition with gradual ingot melting scheme

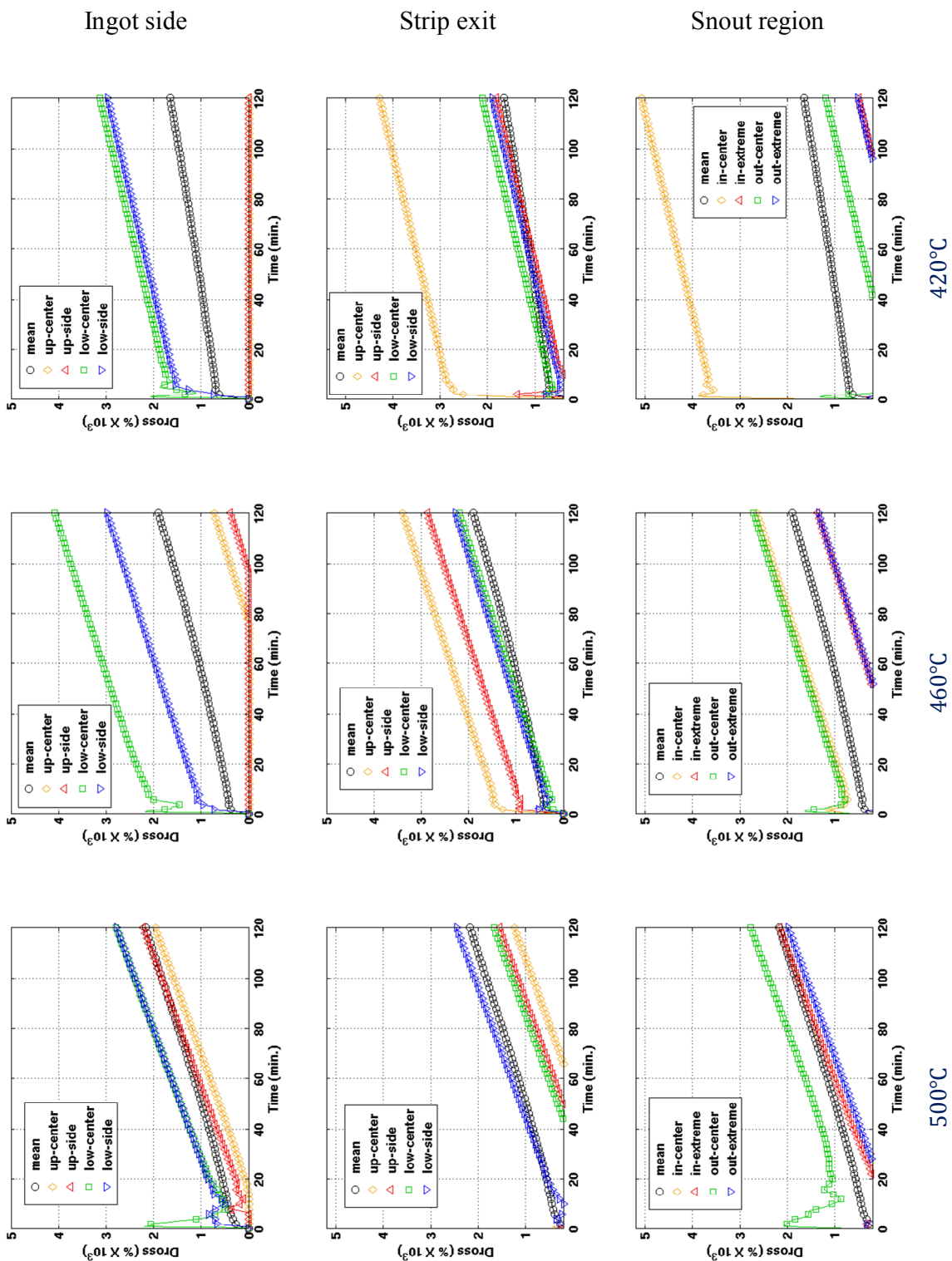


Figure 9: Local dross formation profiles for GI condition with gradual ingot melting scheme

Discussion

It is clear that the strip entry temperature has a strong influence on the galvanizing bath temperature profile. Even though the inductor operation for each case has been adjusted to attain the same overall mean galvanizing bath temperature, the different strip entry temperatures can lead to sufficiently different local temperature fields; especially, at the snout, above the sink roll and at the sides near the inductors. Second, the different strip entry temperatures also induce different Fe dissolution and Al uptake rates. The different rates are shown for the GA and GI operation conditions considered. The combination of the two effects of the strip entry temperature results in considerable differences in the details of dross formation.

Generally, higher dross formation rates are observed wherever the local temperatures are relatively low. The effects of local Fe and Al concentrations are only observed to a lesser degree. The more realistic bath operations considered have little impact on the overall dross formation profile. Thus, local bath temperature control is the key of dross formation management.

On the other hand, higher strip entry temperature condition demands less power to maintain the overall thermal equilibrium. So, it may be beneficial for energy consumption reduction.

ON THE EFFECT OF MN CONTENT OF THE STRIP

Phase diagram of the Al-Fe-Mn-Zn quaternary alloy system

To investigate the effect of Mn content of the strip on the galvanizing bath, it is required to know the zinc-rich corner of the Al-Fe-Mn-Zn quaternary phase diagram near the typical galvanizing bath temperature of 460°C. Gao et al. (2010) experimentally examined the characteristics of the liquid domain of the quaternary phase alloy system at the zinc-rich region at 460°C [16]. Four relevant intermetallic phases are identified and their characteristics are measured.

Based on their work, a numerical phase diagram for the Al-Fe-Mn-Zn quaternary alloy system was developed, which is shown in Figure 10. Expressions for the phase boundaries, however, are not available. Here, they are approximated using spline curves with the experimental data. The obtained numerical phase diagram is rather comparable with the schematic description of the alloy system proposed by Gao et al [16].

The modeling approach for the quaternary phase system is straightforward. But since the data of the quaternary alloy system at temperatures other than 460°C are scarce, it is not possible to construct the numerical phase diagram for the nearby temperatures in similar fashion.

A further challenge for the present investigation is that data of the Mn dissolution rate from the steel strip into the Zn bath is also limited. In other words, even if the phase diagram of the quaternary alloy system is readily available for all the necessary conditions, it would still be non-trivial to locate the composition of the liquid phase of the zinc bath.

As a first approximation, the dissolution rate of Mn may be considered to be the same as that of Fe³. That is,

³ Personal communication with Dr. Daniel Liu (Teck Metals Ltd.)

Mn dissolution rate = Total Fe dissolution rate \times Relative Mn content in the strip
Phase diagram surface for Al-Fe-Mn-Zn

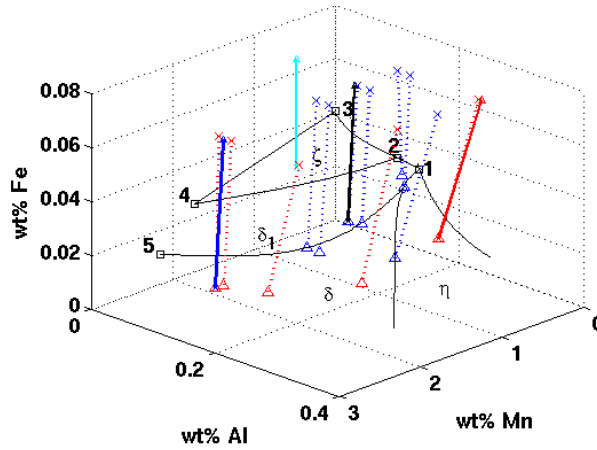


Figure 10: Numerical model of the phase diagram for the quaternary alloy system with experimental data (square – reference data from other works, cross – data for initial solid phases, triangle – data for liquid phases; red - data with single intermetallic phase, blue - data with two intermetallic phases [16]; solid lines - adopted phase characteristics for the intermetallic phases in the present work).

For example, for a steel strip with 20 wt% Mn, the Mn dissolution rate $[Mn]$ is simply:

$$[Mn] = [Fe]_{total} \times 20\%; \quad [Fe]_{new} = [Fe]_{total} \times 80\% \Rightarrow [Mn]/[Fe]_{new} = 25\%$$

The same assumption can be considered for the initial concentration of the galvanizing bath. In particular, if $[Fe]_{bath}$ is at the knee point, $[Mn]_{bath}$ for a steel strip with 20 wt% Mn will be:

$$[Mn]_{bath} = [Fe]_{bath} \times 25\% \approx 0.0277wt\% \times 25\% = 0.00696wt\%$$

Such a very low Mn concentration brings the active regime right next to the Al-Fe-Zn ternary system (Figure 11). This allows some further simplifications to be made on the phase diagram of the alloy system for precipitation formation prediction under typical GA and GI operations.

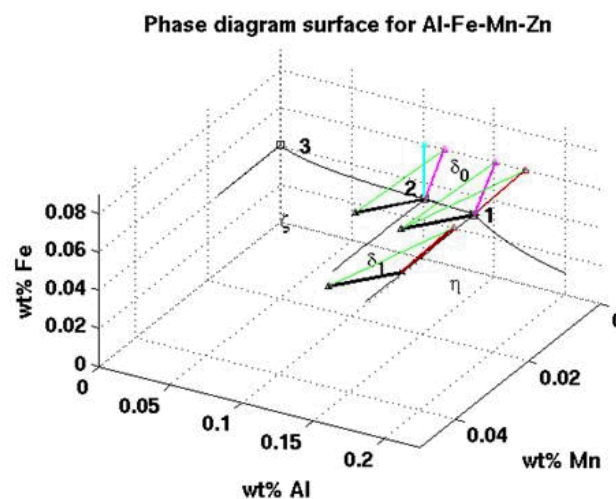


Figure 11: Active region of the phase diagram for very low Mn concentration. Note that the boundary with no Mn represents the Al-Fe-Zn ternary alloy system for conventional steel. First, there are now only three relevant intermetallic phases for dross formation:

1. The η -phase (Fe_2Al_5)
2. The δ_1 -phase ($\text{Fe}(\text{Mn})\text{Zn}_{10}$)
3. The δ_0 -phase (FeZn_{10})

Secondly, the knee point boundary line between the η -phase and the δ_1 -phase can be well approximated using a simple straight line.

Thirdly, such simplification may be assumed to be also valid for the near-by temperatures. This is based on the observation that the function form of the simplified quaternary phase system is essentially the same as that of the well-established Al-Fe-Zn alloy system, which is proven for the temperatures around 460°C. Such approximation permits one to circumvent the lack of data of the quaternary phase system at the near-by temperatures.

Note that in the considerably simplified quaternary phase system (Figure 11), there are still regions containing single, two- and three-intermetallic phases.

Parametric numerical experiment

A parametric study is performed to investigate the potential influence of Mn composition of AHSS on the dross formation characteristics of the galvanizing bath. Three levels of variation are considered for the Mn content in the steel (0.0, 6.0 and 15 wt%) at two different Al bath concentrations (0.12 and 0.16 wt%) and at three different strip entry temperatures (440, 460 and 480°C).

To quantify the potential reduction of Fe dissolution from the strip due to the presence of Mn in the strip (i.e. blockage effect), four levels of Fe dissolution reduction are compared; in particular, with 30%, 57% and 86% reduction as well as without any reduction.

Altogether, 24 study cases are considered. The dross formation rates are determined after the two-hour operation time with the gradual ingot loading scheme. While the different dissolution rates have little influences on the overall dross formation profile, there are considerable impacts on the detail dross formation characteristics.

Dross formation characteristics

Generally, there is larger amount of dross formed for the GA condition than that for the GI condition. This is expected, since first, Mn can substitute as much as 75% in the δ phases formed under the GA condition; whereas, Mn is not so soluble in the η phase formed under the GI condition [16]. Therefore, for the same amount of Fe dissolved into the bath, more dross can be formed under the GA condition. Secondly, the Fe dissolution rate for the GA condition is also higher than that of the GI condition. Lastly, the δ phases are also heavier than the η phase.

The rate of dross formation is observed to be “largely” dependent on the rate of Fe dissolution. The effects of the Mn composition and the reduced Fe dissolution may be combined together by considering the effective Fe dissolution factor per strip entry temperature as:

$$Fe_{dis-overall} = \underbrace{(1 - wt\%Mn) F_{red}}_{Fe\ dis.\ eff.\ factor} Fe_{dis}$$

If the effective Fe dissolution factor is divided by a reference condition, e.g. with 0 wt% Mn and no reduction in the Fe dissolution rate at $T_{strip} = 460^{\circ}C$, the global overall effective Fe dissolution factor can be obtained as follows:

$$Fe_{dis-overall} = \underbrace{(1 - wt\%Mn) F_{red}}_{Fe\ diss.\ eff.\ factor} Fe_{dis-T} / Fe_{dis-460}$$

It is found that the global dross formation rate (ordinate) correlates very well with the global overall effective Fe dissolution factor (abscissa). Using the same reference condition as the benchmark for the global dross formation rate, the dross formation characteristics for the GI bath condition are summarized in Figure 12. The slope can be described linearly as:

$$Dross_{0.16} \approx 20.0 + 0.8 Fe_{dis-overall}$$

With similar Fe dissolution rate, the results suggest that the amount of dross formation is less for higher strip entry temperature. This is especially true when the overall Fe dissolution rate is low. As the Fe dissolution rate increases, the difference in dross formation rate decreases among the different strip entry temperatures.

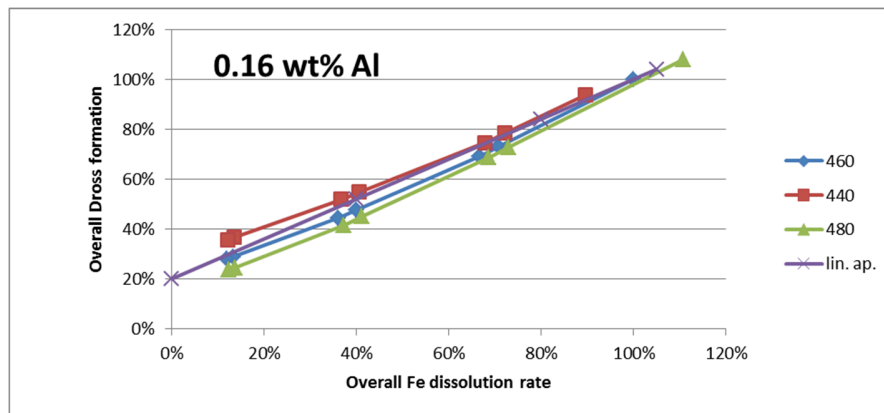


Figure 12: Overall dross formation verse overall Fe dissolution rate for the GI condition.

The dross formation characteristics for the GA condition are summarized in Figure 13. The corresponding linear relation is:

$$Dross_{0.12} \approx 20.0 + 1.8 Fe_{dis-overall}$$

Similarly, at lower overall Fe dissolution rate, the dross formation is lower for a higher strip entry temperature. Notice also that the slopes for both δ phases are comparable and there is approximately a factor of two between the two phases, consistence with the modelling assumption employed for the Mn-Fe substitution.

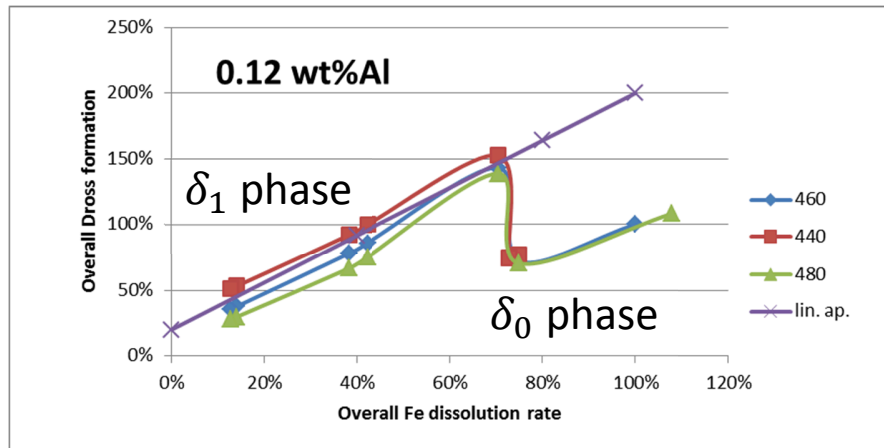


Figure 13: Overall dross formation verse overall Fe dissolution rate for the GA condition

Discussion

These results demonstrate that the Fe dissolution rate has a great impact on the amount of dross formed. Often, the control programs for galvanizing bath consider the steel strip simply as IF steel grade in their computations. This can certainly introduce errors in the prediction and the corrective actions. As the compositions of the modern steel products become increasingly complex, the differences in the Fe dissolution rate should be carefully observed and adjustments made to operating practice as needed.

CONCLUSIONS

In the present work, the effects of the strip entry temperature and Mn content on the galvanizing bath management are investigated numerically using a well-validated galvanizing bath model. The impacts are quantified in terms of the bath flow, temperature and compositional characteristics, as well as the dross formation patterns for all test scenarios.

It is concluded that local bath temperature must be properly regulated to minimize the local dross formation rate. Higher strip entry temperature will result in much less dross around the strip, but it may still lead to higher overall dross formation. It is noted that a higher strip entry temperature requires less inductor power to maintain the overall energy balance of the bath and may be beneficial for energy consumption reduction.

On the other hand, higher strip Mn content could result in significantly more dross, particularly at the GA condition. Lastly, the Fe dissolution rate from the steel strip has great impacts on the dross formation and such factor should be carefully considered in the bath management analysis.

ACKNOWLEDGEMENT

The first author would like to thank Dr. Daniel Liu from Teck Metals Ltd. for the insightful discussions and providing the strip Fe dissolution and Al uptake data. The authors would also like to acknowledge the International Zinc Association, the sponsors of the Galvanized Autobody Partnership program ZCO-71 and the Advanced Manufacturing and Design Systems program of NRC for making this work possible.

REFERENCES

- [1] S. Keeler and M. Kimchi, Eds., “Advanced High Strength Steel (AHSS) Application Guidelines.” World Steel Association, 2014.
- [2] F. Ajersch, M. Gauthier, and C. Binet, “Kinetics of continuous galvanizing process,” in *Fundamentals of metallurgical processing: proceedings of James M. Toguri Symposium - MetSoc 39th Annual Conference of Metallurgists of CIM, August 20 - 23, 2000, Ottawa, Ontario, Canada*, G. Kaiura, C. Pickles, T. Utigard, and A. Vahed, Eds. Montreal: Canad. Inst. of Mining, Metallurgy and Petroleum, 2000, pp. 161–178.
- [3] F. Ilinca, J.-F. Héту, and F. Ajersch, “Three-dimensional numerical simulation of turbulent flow and heat transfer in a continuous galvanizing bath,” *Numer. Heat Transf. Part Appl.*, vol. 44, no. 5, pp. 463–482, 2003.
- [4] F. Ajersch, F. Ilinca, and J.-F. Héту, “Simulation of Flow in a Continuous Galvanizing Bath: Part I. Thermal Effects of Ingot Addition,” *Metall. Mater. Trans. B Process Metall. Mater. Process. Sci.*, vol. 35, no. 1, pp. 161–170, 2004.
- [5] F. Ajersch, F. Ilinca, and J.-F. Héту, “Simulation of Flow in a Continuous Galvanizing Bath: Part II. Transient Aluminum Distribution Resulting from Ingot Addition,” *Metall. Mater. Trans. B Process Metall. Mater. Process. Sci.*, vol. 35, no. 1, pp. 171–178, 2004.
- [6] F. Ajersch, F. Ilinca, and F. E. Goodwin, “Numerical simulation of flow, temperature and composition variation in the snout and sink roll region of continuous galvanizing baths,” in *Materials Science and Technology Conference and Exhibition 2013, MS and T 2013*, 2013, vol. 2, pp. 1145–1152.
- [7] F. Ilinca, F. Ajersch, C. Baril, and F. E. Goodwin, “Numerical simulation of the galvanizing process during GA to GI transition,” *Int. J. Numer. Methods Fluids*, vol. 53, no. 10, pp. 1629–1646, 2007.
- [8] K. R. Yu, F. Ilinca, and F. E. Goodwin, “Numerical simulation of the effect of strip entry temperature on continuous galvanizing bath management and dross formation,” in *AISTech - Iron and Steel Technology Conference Proceedings*, 2016, vol. 2, pp. 2043–2053.
- [9] A. R. Marder, “Metallurgy of zinc-coated steel,” *Prog. Mater. Sci.*, vol. 45, no. 3, pp. 191–271, 2000.
- [10] F. Ilinca and D. Pelletier, “Positivity preservation and adaptive solution for the k- ϵ model of turbulence,” *AIAA J.*, vol. 36, no. 1, pp. 44–50, 1998.
- [11] N.-Y. Tang, “Refined 450°C isotherm of Zn-Fe-Al phase diagram,” *Mater. Sci. Technol.*, vol. 11, no. 9, pp. 870–873, 1995.
- [12] N.-Y. Tang, “Determination of liquid-phase boundaries in Zn-Fe-Mx systems,” *J. Phase Equilibria*, vol. 21, no. 1, pp. 70–77, 2000.
- [13] L. P. Franca and S. L. Frey, “Stabilized finite element methods: II. The incompressible Navier-Stokes equations,” *Comput. Methods Appl. Mech. Eng.*, vol. 99, no. 2–3, pp. 209–233, 1992.
- [14] Y. H. Liu and N.-Y. Tang, “Computer modeling of aluminium uptake and iron dissolution in galvanizing and galvannealing,” in *Galvatech '04: 6th International Conference on Zinc and Zinc Alloy Coated Steel Sheet - Conference Proceedings*, 2004, pp. 1155–1164.
- [15] Y. H. Liu, “Experimental Validation of Computer Simulation of Aluminum Pickup and Iron Dissolution in Galvanneal and Galvanize Production,” in *Galvatech 2015 Proceedings*, 2015, pp. 545–552.
- [16] N. Gao, Y. H. Liu, and N.-Y. Tang, “An experimental study of the liquid domain of the Zn-Fe-Al-Mn quaternary system at 460 °C,” *J. Phase Equilibria Diffus.*, vol. 31, no. 6, pp. 523–531, 2010.